Hydraulic artificial muscles

Rashi Tiwari*, Michael A Meller*, Karl B Wajcs, Caris Moses, Ismael Reveles and Ephrahim Garcia

Abstract

This article presents hydraulic artificial muscles as a viable alternative to pneumatic artificial muscles. Despite the actuation mechanism being similar to its pneumatic counterpart, hydraulic artificial muscles have not been widely studied. Hydraulic artificial muscles offer all the same advantages of pneumatic artificial muscles, such as compliance, light weight, low maintenance, and low cost, when compared to traditional fluidic cylinder actuators. Muscle characterization in isometric and isobaric conditions are discussed and compared to pneumatic artificial muscles. A quasi-static model incorporating the effect of mesh angle, friction, and muscle volume change throughout actuation is presented. This article also discusses the use of hydraulic artificial muscles for low-pressure hydraulic mesoscale robotic leg.

Introduction

The McKibben artificial muscle actuator, named after its inventor Joseph L McKibben, has been commonly used in robotics systems (Chang and Lilly, 2003; Ho et al., 2000; Lilly, 2003; Noritsugu and Tanaka, 1997; Tondu et al., 2005; Vanderborght et al., 2004, 2006; Varga and Moucka, 2009; Wisse and Frankenhuyzen, 2003; Yoshinada et al., 1991), prosthetics or artificial limbs (Ferris et al., 2005; Lee and Shimoyama, 1999; Nakamura et al., 2003; Waycaster et al., 2011), and morphing (Chen et al., 2011; Kothera et al., 2010; Wereley et al., 2009; Woods et al., 2011; Yerkes and Wereley, 2008). Typically, these muscles are pneumatically driven, have large force-to-weight and force-to-volume ratios and are highly compliant.

McKibben muscles have some analogous characteristics to skeletal muscle such as functionality only in tension mode, decreasing force with increasing contraction (Tondu and Lopez, 1997), and the need for an antagonistic pair for double-acting motion. Due to their resemblance to biological muscles and pneumatic operation, they are commonly referred as pneumatic artificial muscles (PAMs).

Traditionally, PAMs are composed of an inner elastomeric tube, an outer helically wound braided sleeve, one fluid plug, one fluid port, and tube clamps to hold the other components together. When pressurized fluid is supplied through the fluid port, it causes the inner bladder of the artificial muscle to expand radially. Normally, the inner tube would want to expand axially as well, but there is a pretensioning of the inner tube involved in the manufacturing process that eliminates this. As the bladder expands radially, it pushes against the outer braided sleeve. This causes the whole muscle to contract axially, or produce tension, or both (Chou and Hannaford, 1996). Various modifications of PAMs like pleated muscles (Daerden, 1999; Daerden and Lefeber, 2001), sleeved bladder muscles (Beullens, 1989; Winters, 1995), and netted muscles (Immega, 1986, 1987; Yarlott, 1972) have been reported in the literature (Fluidic Muscle DMSP/MAS, n.d.; Shadow Robot Company, n.d.).

The typical maximum pressure of operation has been reported to be ranging from 500 to 800 kPa. This maximum pressure is limited by the strength of material and need for compliance in the muscle. The stroke of artificial muscles tends to be directly dependent only on the length of the muscle. Most artificial muscles have a maximum stroke between 25% and 40% of their maximum active length; however, some muscle variants have strokes of over 50% of their maximum length (Daerden and Lefeber, 2002). Due to highly nonlinear dynamic behavior, PAMs are difficult to control and model.

Laboratory of Intelligent Machine Systems, Cornell University, Ithaca, NY, USA

(* Authors with equal contribution)

Corresponding author:
Ephrahim Garcia, Mechanical and Aerospace Engineering, 224 Upson Hall, Cornell University, Ithaca, NY, USA.
Email: EG84@cornell.edu

The research reported in this article aims to extend the capability of traditional artificial muscles as hydraulic actuators. Though the use of PAMs with hydraulic fluid may result in increased weight, it is expected to benefit the research on exoskeletons (Wigging et al., 2011) and mesoscale underwater robots where the surrounding water could be used as a reservoir. Also, the use of bulky compressors can be avoided in hydraulic artificial muscles (HAMs), thus making compact design possible. Additionally, using different working fluid like water or oil could result in HAMs of different stiffness, which is specifically beneficial for exoskeleton design and control. Focchi et al. (2010) compared the use of air and water for artificial muscle. They reported that stiffness increases linearly with the contraction of the muscle.

Characterization tests in isometric and isobaric modes, using in-house mesoscale muscles, are reported in this article to provide insight into the muscle's behavior in quasi-static conditions. In-house muscles were fabricated for these tests. A static nonlinear model to predict muscle performance is also reported. HAM application in a robotic leg is also presented.

HAMs

Recently, researchers have been looking into using artificial muscles with hydraulic working fluid. Ryu et al. (2008) developed microscale HAMs of diameter 2 mm for use in haptic gloves that was capable of generating a force up to 5 N. Ku and Bradbeer (2006) tested artificial muscles with water as the working fluid in both static and dynamic conditions, demonstrating the possibility of utilizing liquids as the working fluid. Muscles of three different diameters were actuated at three different pressures of 100, 200, and 300 kPa in their study. Recently, Sodano and Rotinat-Libersa (2011) reported the application of artificial muscles as hydraulic actuators for millimeter scale robot development. Robinson et al. (2011) reported the use of in-house 2-inch outer diameter muscles fabricated using silicon bladder in a robotic arm of length in the order of human arm.

Quasi-static model

Due to the hysteresis, bladder nonlinearities, and compliance, the control of an artificial muscle becomes difficult. Hence, there is a need for a model to take these parameters and their effects into account. Many models exist in the literature (Caldwell et al., 1993; Davis et al., 2003; Ku et al., 2008; Vo-Minh et al., 2010) and can be broadly classified into geometric models (Chou and Hannaford, 1996; Klute and Hannaford, 2000; Schult, 1961; Tondu and Lopez 2000) and phenomenological models (Reynolds et al., 2003). The static model reported by Chou and Hannaford (1996), which is most widely used, is based on the assumption that the tubing in the artificial muscle remains cylindrical on inflation. Tondu and Lopez (2000) developed a static model that takes into

account the end effects due to capping. Wickramatunge and Leephakpreeda (2010) compared the behavior of PAMs to a spring whose stiffness is dependent on actuation pressure and stroke. Vo-Minh et al. (2009) later developed a lumped parameter quasi-static model to incorporate hysteresis that could also be used for controlling PAMs.

In general, most of the models in the literature are based on approximation and correction factors and have been developed for PAMs. There are numerous parameters like braid angle, braid length, friction, the viscoelastic nature of the bladder, and noncylindrical inflation of the bladder due to end caps that have been neglected. These end effects are even more pronounced in mesoscale HAMs. The models discussed in this section aim to account for the many characteristics of artificial muscles and their static operation. The model laid out in this article is based on the static model by Chou and Hannaford (1996). However, the model by Chou and Hannaford (1996) was modified to incorporate volume change and friction due to mesh for a more accurate prediction of the muscle behavior.

In order to find the force output from the artificial muscles, the principle of "virtual work" was employed. This states that the work out is equal to the work in. Thus, the work done by increasing the volume of the muscle is equal to the work done by the muscle as it contracts and changes length]

$$W_{out} = W_{in} \tag{1}$$

where

$$\begin{aligned} W_{out} &= -FdL \\ W_{in} &= PdV \end{aligned} \tag{2}$$

Hence

$$F = -P\frac{dV}{dL} \tag{3}$$

where P is the pressure of the fluid inside of the muscle, F is the force output by the muscle, dV is the change in volume, and dL is the change in length.

The length and volume of the muscle are defined in terms of mesh angle, θ, and the force is found by differentiating both length and volume with respect to θ.

$$F = -P\frac{dV/d\theta}{dL/d\theta} \tag{4}$$

To understand the geometry, imagine that you stretch out one strand of mesh along θ (Figure 1). The length and volume of the muscle is defined in terms of mesh angle, θ

$$\begin{aligned} L &= b\,\cos\,\theta \\ D &= \frac{b\,\sin\,\theta}{n\pi} \\ V &= \pi\left(\frac{D}{2}\right)^2 L \end{aligned} \tag{5}$$
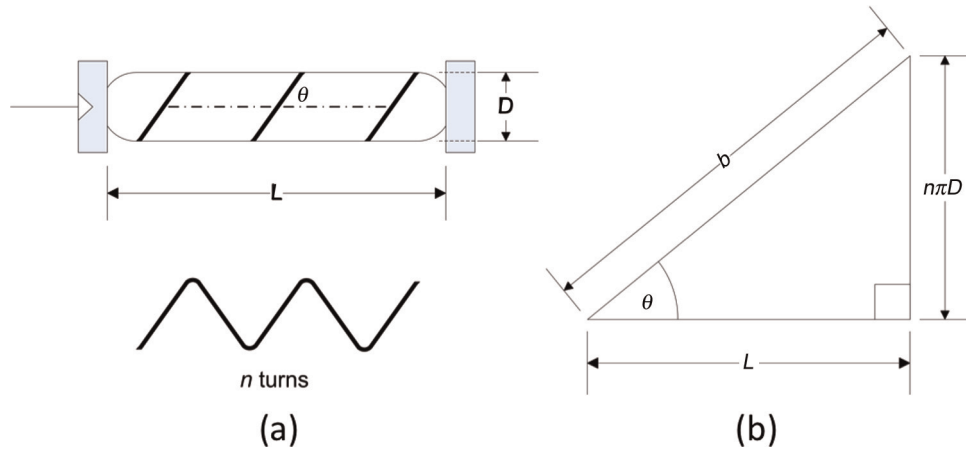
Figure 1. (a) Muscle model parameters of the entire muscle and (b) one unraveled strand of mesh (b = length of one strand of mesh and n = number of times one strand wraps around the muscle).

where, n is the number of turns of each strand of the mesh and b is the length of one strand of mesh. Differentiating the length and volume with respect to θ, the force, F, can then be calculated as

$$F = \frac{Pb^2\left(2\cos^2\theta - \sin^2\theta\right)}{4\pi n^2} \quad (6)$$

It should be noted that this model currently does not take into account the thickness of the bladder and the viscoelastic behavior of the tube. This is because the thickness of the bladder does not seem to have much impact on the actuation characteristics of the muscle when the bladder wall is thin (Chou and Hannaford, 1996), and the viscoelasticity will have more effect in the dynamic condition. However, different volume shapes and the thread friction will be incorporated in our quasi-static model of the muscles.

Model modifications

Volume. On actuation, the muscle starts to radially expand in the middle. At maximum contraction, the bladder expansion can be assumed to be composed of a cylindrical portion in the middle and a conical portion near the end cap, as shown in Figure 2. The model presented in this article incorporates this volume change in terms of cylinder-to-cone ratio. The volume of cone to

cylinder is in turn dependent on the pressure in the muscle. The muscle volume change from completely cylindrical (when fully extended) to both conical (30%) and cylindrical (70%) when fully contracted is used in the model. The total volume was modified as

$$V = V_{cone}x + V_{cylinder}(1 - x) \quad (7)$$

where V_{cone} is the volume contribution of cone and $V_{cylinder}$ is volume contribution of cylinder. The factor x is in turn dependent on the elongation of the muscle.

$$x = \frac{0.3}{E_{max}}E$$
$$E = \frac{L_{max} - L}{L_{max}} \quad (8)$$

where L_{max} is the maximum length when the muscle is fully stretched and E_{max} is the contraction ratio when $L = L_{min}$. A correction factor was included in the model to account for the modifications that still need to be made to incorporate nonlinearities largely due to the viscoelastic tube inside of the muscle.

Friction. Another important parameter that should be accounted for in the model is hysteresis between lengthening and shortening. The hysteresis that occurs can mostly be attributed to the Coulomb friction that exists
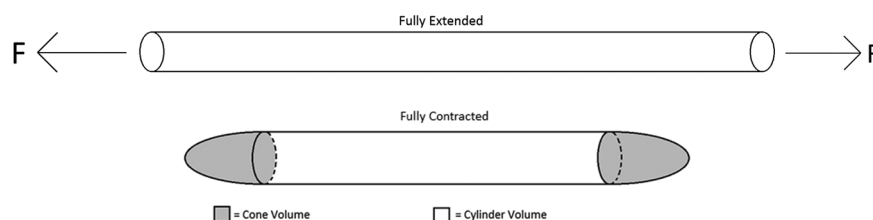

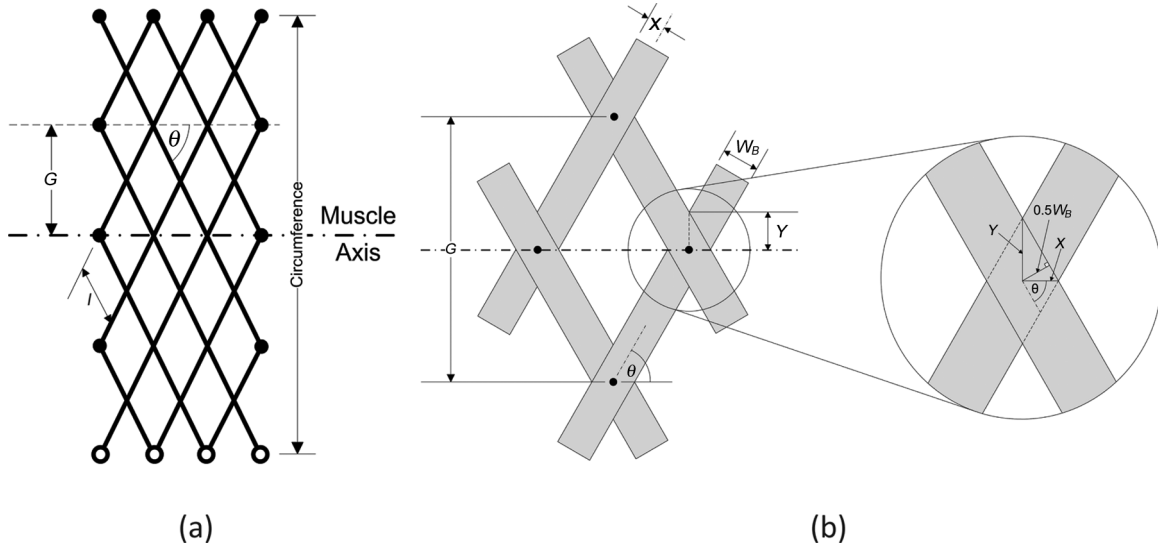**Figure 2.** Illustration showing noncylindrical muscle actuation.

Figure 3. (a) Unrolled mesh and (b) one trapezoid of mesh (G is the distance between two nodes, θ is the angle between the braid strands and the axis of the muscle, W_B is the thickness of a strand of mesh material, and D_o is the diameter of the muscle when $\theta = 90°$).

between the braided mesh and the inner tube, as well as between the braided mesh and itself (Tondu and Lopez, 1997). Some research groups have created and reported on other alternative versions of artificial muscles that reduce hysteresis as well as increase the contraction abilities of the actuators (Daerden and Lefeber, 2002; Immega and Kukolj, 1990; Paynter, 1998). However, limited availability of these muscles in the market reduces their application.

The frictional force calculation similar to the one by Davis and Caldwell (2006) is employed. The coordinate system and the variables used in the derivation are explained in Figure 3.

When the mesh angle, θ is 90°, the circumference, C, is

$$C = 2lN_C \tag{9}$$

where, N_C, is the number of nodes (Figure 3) around a muscle. The circumference can also be calculated as

$$C = \pi D_O \tag{10}$$

where D_o, is the diameter of the muscle when the mesh angle is 90°. Equating the above equations for circumference to each other, the length of the sides of a trapezoid, l, is calculated as

$$l = \frac{\pi D_O}{2N_C} \tag{11}$$

Using Figure 3, the distance between two mesh nodes, G, and the variables X and Y, can be calculated as

$$G = 2l \sin \theta \tag{12}$$

$$X = Y \cos \theta \tag{13}$$

$$2X = W_B, \; Y = \frac{W_B}{2 \cos \theta} \tag{14}$$

where W_B is the thickness of individual mesh strand. When the braid angle is at its smallest, θ_{min}

$$G = 2Y \tag{15}$$

Equating equations (12) and (15) and plugging in equations (11) and (14), θ_{min} is

$$\theta_{min} = \frac{1}{2} \sin^{-1} \left(\frac{2W_B N_C}{\pi D_O} \right) \tag{16}$$

The frictional force is dependent on f_S, the coefficient of friction, and $S_{contact}$, the total area of overlapping mesh.

$$F_{friction} = f_S S_{contact} P \tag{17}$$

To find $S_{contact}$, we must first find the area of one overlapping mesh (S_{one}) and the number of overlapping strands in the entire muscle ($N_{contact}$).

$$S_{contact} = S_{one} N_{contact} \tag{18}$$

The area of contact can be calculated using trigonometric relationships as shown below (Figure 3(b)).

$$\tan \theta = \frac{x}{y} \tag{19}$$

$$\sin \theta = \frac{W_B}{2y} \tag{20}$$

$$S_{one} = 2xy \tag{21}$$

$$S_{one} = \frac{W_B^2}{2 \cos \theta \sin \theta} \tag{22}$$

At θ_{min}, the diameter is D_{min}, and the length is L_{max}. There are no gaps in the mesh, so the total surface area is $S_{contact}$

$$\text{Surface area} = \pi D_{min} L_{max} = S_{one} N_{contacts} \quad (23)$$

Using the diameter and the length defined previously, plug θ_{min} in to find D_{min} and L_{max}. Solving for $N_{contact}$

$$N_{contacts} = \frac{2b^2 \sin^2 \theta_{min} \cos^2 \theta_{min}}{n W_B^2} \quad (24)$$

The total area of the overlapping strands, $S_{contact}$, can be determined as

$$S_{contacts} = \frac{b^2 \sin^2 \theta_{min} \cos^2 \theta_{min}}{n \sin \theta \cos \theta} \quad (25)$$

An increase in the overlapping area results in increased strand friction, hence an increase in muscle nonlinearity as well. The values of different variables used in this article are listed in Table 1.

The model also clearly indicates that both PAMs and HAMs theoretically should provide the same force output, as this is independent of operating fluid in static operation. In the following section, experimental characterization of HAMs and their comparison with PAMs are discussed.

Characteristics of small-sized HAM

Experimental setup

In order to gain a better understanding of artificial muscles, the muscles reported in this article were manufactured in-house using off-the-shelf components and have strokes ranging from 6.35 mm (¼ of an inch) to a couple millimeters. One of these in-house manufactured artificial muscles and the components it consisted of can be seen in Figure 4. For the in-house artificial muscles, the maximum active length was measured from the inside of one tube clamp to the other when the muscle is fully stretched.
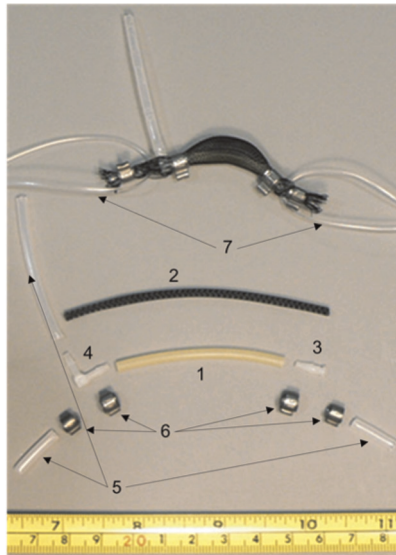
All muscles were constructed using the same materials, so the following muscle details applied to all the muscles used in the research:

Bladder: 1.5875 mm (1/16″) inner diameter, 0.7938 mm (1/32″) thickness (therefore 3.1750 mm (1/8″) outer diameter).
Braid: 3.1750 mm (1/8″) inner diameter at its thinnest (so when muscle is stretched out).
Diameter: Outer diameter is around 3.1750 mm (1/8″) at the smallest and should increase to about 6.35 mm (1/4″) at the largest.

Experiments were conducted in order to statically characterize the in-house mesoscale HAMs and PAMs.

Table 1. Table listing the some of the material properties.

Variables	Value	Units
Length of one side of a trapezoid of mesh, l	1	mm
Length of one strand of mesh, b	25	mm
Number of turns one strand makes, n	1	—
Thickness of a mesh strand, W_B	0.25	mm
Number of nodes around a muscle, N_C	18	—
Diameter of muscle when $\theta = 90°$, D_o	7.958	mm
Friction coefficient, f_s	0.1	—

1	Soft latex inner rubber tube
2	Expandable polyester braided mesh sleeve
3	Single-barbed nylon tube fitting plug
4	Single-barbed nylon tube fitting 90° elbow port
5	Polyurethane tubing
6	Stainless steel pinch tube clamps
7	Tendon-like attachment

Figure 4. Diagram of in-house artificial muscle components.
1: soft latex inner rubber tube; 2: expandable polyester braided mesh sleeve; 3: single-barbed nylon tube fitting plug; 4: single-barbed nylon tube fitting 90° elbow port; 5: polyurethane tubing; 6: stainless steel pinch tube clamps; 7: tendon-like attachment.
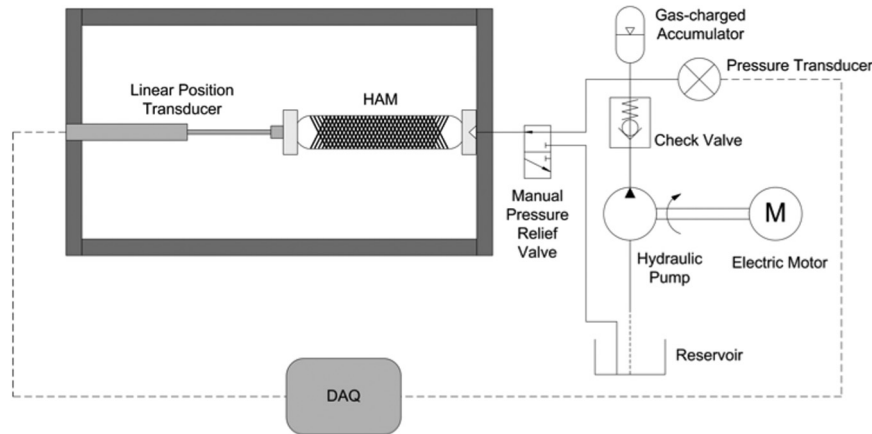
Figure 5. Test rig for free-stroke measurement (solid lines denote fluid lines, while large dashed lines are electrical connections). DAQ represents data acquisition system.

Tests were performed under isometric and isobaric conditions, using an Instron 1125 and Bose Electroforce, respectively. The isometric experiments were designed to measure the maximum force output of the muscles at various pressures, keeping the muscle length constant at its longest position. Forces for the isometric tests were recorded using a Load Star Sensors, iLoad Digital USB load cell. For the isometric experiments, each muscle was inserted into the Instron 1125 and stretched to its full length. An initial preload is necessary due to the stretching of the inner bladder in manufacturing. Once this was done, the load cell was calibrated. Each muscle was then inflated to pressures ranging from 0 to 100 psi in increments of 20 psi at each stage. After reaching a pressure of 100 psi, the system was reset, and the procedure was repeated two more times for a total of three trials with each muscle.

Isobaric tests were performed to measure force output from the muscles on elongation/contraction at a series of pressures that were held constant for each experiment. The muscles were tested at pressures ranging from 60 to 100 psi. For the isobaric tests, only muscles 22 mm in length were used.

Experiments were performed to measure free stroke and blocking force of the muscles. Free stroke is defined as the stroke with no load attachment, and blocking force is the maximum force generated by the muscle with no displacement. For the free-stroke measurements, the muscles were mounted horizontally, fixed at one end of the rig and attached to a linear position transducer (Bourns Inc., 101.6 mm-5 kΩ) at the other, as shown in Figure 5. Muscle is stretched to its maximum length at the starting of the experiment. The pressure was increased from 0 to 100 psi by increments of 20 psi. The data was read from the linear potentiometer via a data acquisition unit (USB-1608FS, Measurement Computing). Each muscle was tested for a total of three times.

In the isometric and free-stroke experiments, three different lengths of muscles were tested with two

Table 2. Table of muscle lengths.

Tests	Muscle length (mm)
Isometric and free stroke	80
	120
	160
Isobaric	22

different muscles for each length. Muscle active lengths are listed in Table 2. The same sets of muscles were used for both hydraulic and pneumatic testing.

Results

The results of isobaric, isometric, and free-stroke experiments are shown in Figures 6 to 8. Although care was taken to minimize any discrepancies, some variations could be due to fabrication of the different muscles, as well as the different tubing and fittings used between the pneumatic and hydraulic setups. Isometric tests were performed using three different muscle sizes and four muscles of each size. The results clearly show that the force increases with increasing pressure as well as increasing length (Figure 5). Our test results show that the force output is indeed dependent on length, though to a lesser degree than its pressure dependence. The output from both PAM and HAM was similar as predicted by the model.

Another variable that plays an important role is the threshold pressure, that is, the minimum pressure required to actuate a muscle. Each muscle needs to be actuated beyond its threshold pressure in order to perform work. Due to the nonlinearity of the tubing, some variation in threshold pressure in different muscles of the same size was observed. In addition, HAMs were observed to have some remnant strain on deflation.

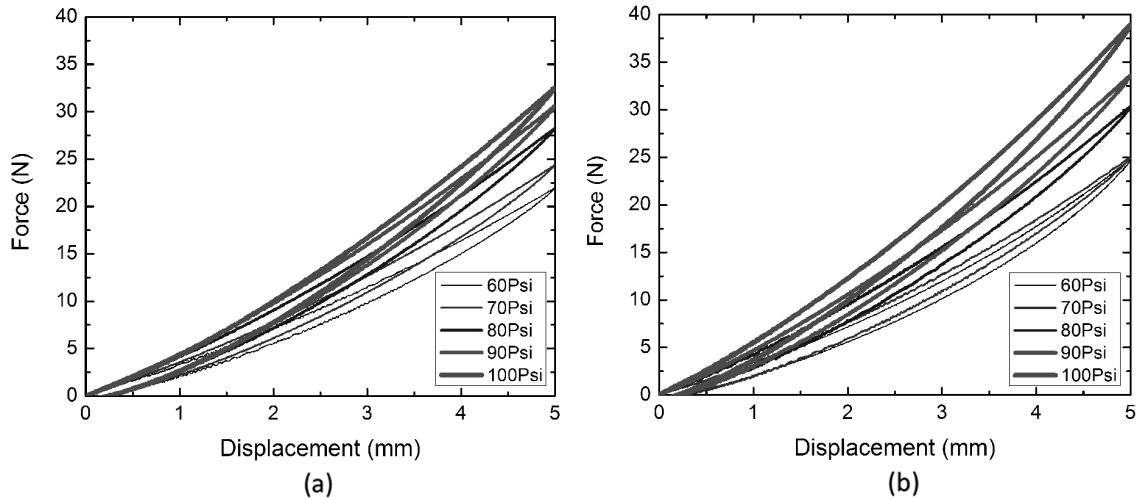Figure 8 compares PAMs and HAMs in terms of free stroke and blocking force. Muscles of size 80, 120,

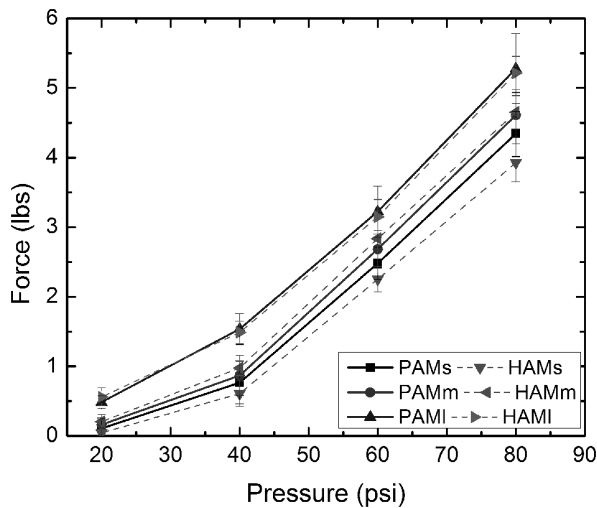**Figure 6.** Isobaric tests performed using (a) PAM and (b) HAM of length 22 mm.

Figure 7. Isometric tests performed using 80-mm (subscript "s"), 120-mm (subscript "m"), and 160-mm (subscript "l") PAMs and HAMs.

and 160 mm show an increase in both blocking force and free stroke with an increase in pressure. The free stroke in the case of HAMs was observed to be marginally higher than PAMs. This could be due to better pressure control in HAMs due to the use of an accumulator.

It should also be noted that since the muscles used in this research are small, parameters like end effects due to clamping in the muscles, friction, and noncylindrical inflation of the tube has more pronounced effects on the muscle characteristics. The static model predicts identical force output from the muscles irrespective of the operating fluid. HAM model modified with friction between mesh strands and to a more realistic noncylindrical shape (resembling a cone) was observed to improve the predictability of the model. Figure 9 compares model with experimental data for isobaric tests, which were performed to measure force output from
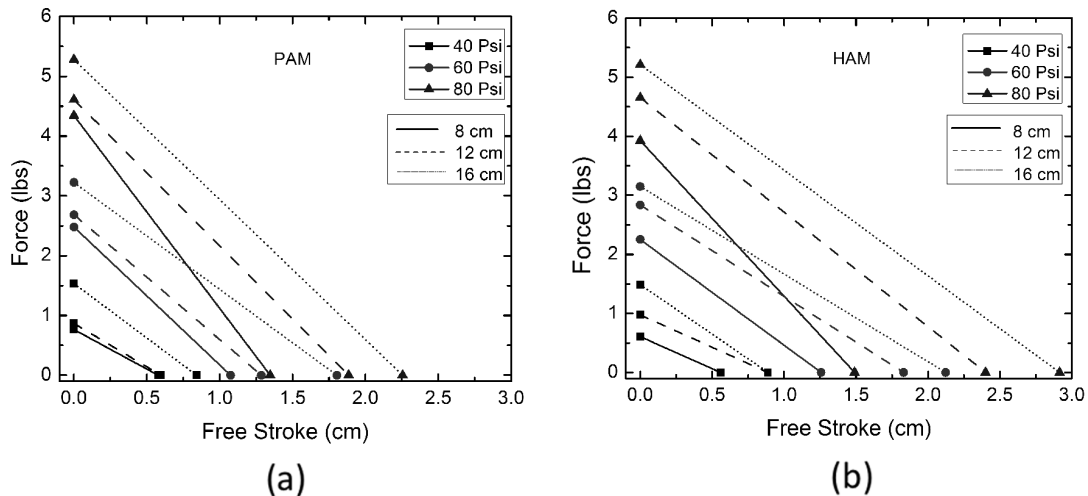

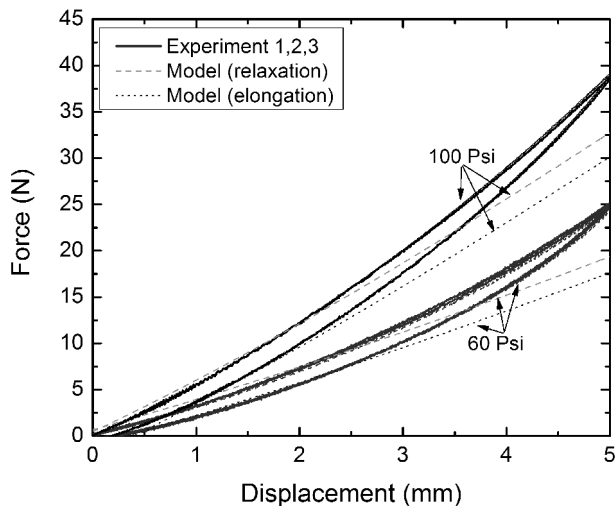**Figure 8.** Blocking force and free stroke for (a) PAM and (b) HAM.

Figure 9. Comparing static model predictions with experimental data in isobaric conditions using HAMs.

the muscles on elongation and relaxation at a series of pressures that were held constant for each experiment. Though the model predicts identical output from the PAM and HAM actuators, the experimental results show marginally better performance from the hydraulic actuators.

Currently, the model does not take into account the nonlinear modulus term resulting from the viscoelastic nature of the tube. Though the viscoelastic behavior may not be that prominent in static tests, it will most likely have large effect on the dynamic nature of the muscle.

Application of HAMS

The same valve that is often used for controlling double-acting cylinders, a 4/3 directional control valve, can actually be used for controlling an antagonistic pair of HAMs as well. These valves are typically used for sending pressurized fluid to both sides of the piston of a double-acting cylinder (chamber A, piston side, and chamber B, rod side) to achieve motion in both directions (Rabie, 2009). It can instead be used to control the fluid flow to both muscles of an antagonistic pair.

As stated previously, appropriately sized HAMs arranged in antagonistic pairs could conveniently be used to replace the existing double-acting cylinders. This would reduce the actuator weight by 84% and would provide a mesoscale robot with more biological motion. Figure 10 shows the two-degree-of-freedom (DOF) leg test rig with HAMs, which is discussed in the following.

The system uses the same one pump and accumulator setup. The leg pieces were fabricated to accommodate the HAMS, which were produced in-house. Two servos actuate the spool valves to control the position of the legs. Each spool valve controls one of the antagonistic pairs of HAMS, either controlling the thigh or
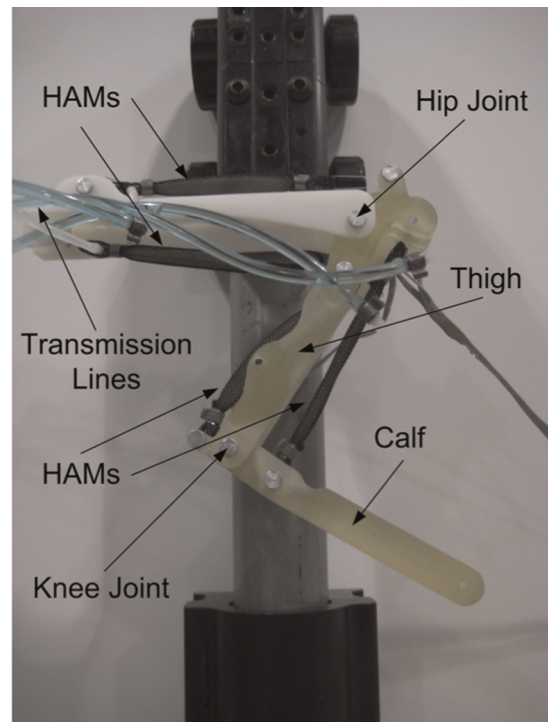

Figure 10. HAM-actuated, two-DOF leg test stand.
HAM: hydraulic artificial muscles; DOF: degree of freedom.

the calf of the leg. The leg is controlled by an Atmel Atmega32 microcontroller using an open-loop controller. The controller sets the position of the valve to fully inflate one of the two HAMS in the antagonistic pair, while venting the other HAM. After a given amount of time, the controller toggles the position of the valves, moving the leg. The four positions that the HAM-actuated leg is toggled between can be seen in Figure 11. It switches between fully contracted and extended for each leg segment in a walking gait motion.

At both the hip and knee joints, there is a conductive plastic rotary potentiometer. The potentiometer at the hip joint measures the angle of the thigh with respect to horizontal. The potentiometer at the knee joint senses the angle between the thigh and the calf. In Figure 11, the measured joint angle data for the walking gait trajectory that was prescribed are shown.

Discussion and conclusion

Both isobaric and isometric tests show similar performance from PAMs and HAMs. This is because the static force output is dependent on the construction of the muscle, position of the muscle, and the operating pressure. The static characteristics should be independent of operating fluid. The static force output from HAM is mostly a function of muscle dimensions, the operating pressure, and what part of its stroke it is in. HAM's static force increases proportionally as pressure is
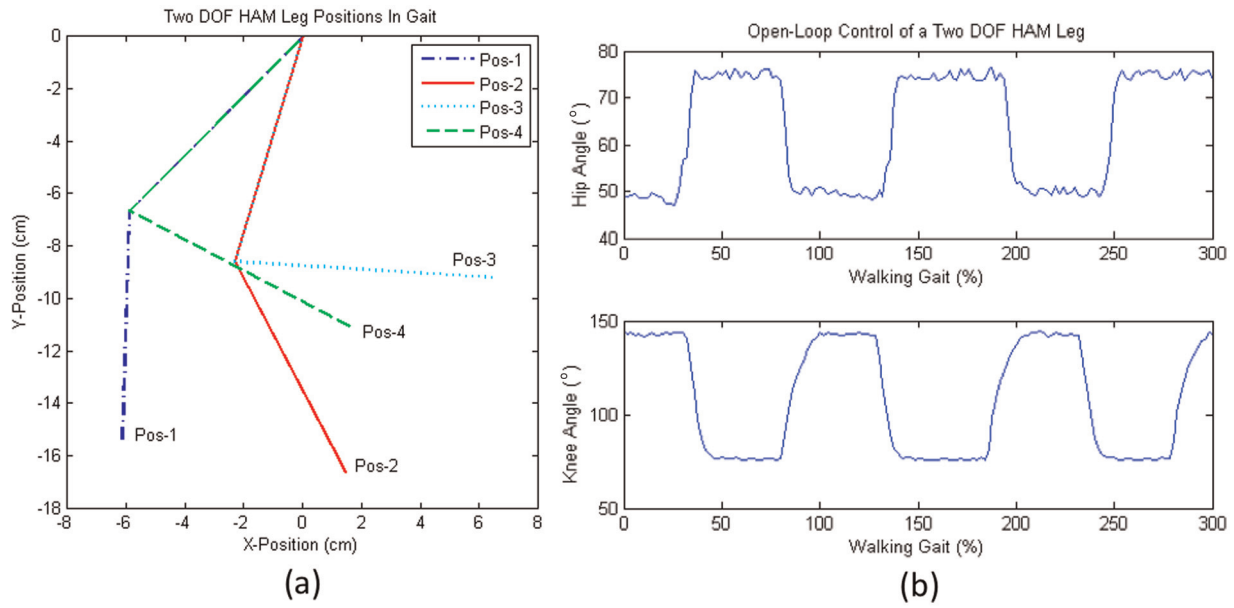
Figure 11. (a) The four positions that are toggled between and (b) the joint angle data from the open-loop control of the HAM-actuated leg.

increased. This is true of traditional cylinder actuators as well. However, one main difference in the operation of the two is that the force a HAM creates is dependent on where it is in its stroke, while a hydraulic or pneumatic cylinder outputs approximately the same force regardless of its position. The static force an artificial muscle can produce increases with decreasing contraction ratio (Tondu and Lopez, 1997). In other words, the maximum static force a muscle can create occurs at its fully stretched position, and this decreases all the way down to zero when the muscle is at its fully contracted state. The muscle acts essentially like a variable stiffness, nonlinear spring, where its "resting" position is when the muscle is fully contracted. The model presented in this work could be modified to incorporate the effect of variable stiffness by using technique developed by Shan et al. (2009) and Philen (2011).

HAMs are most similar to single-acting cylinders, as both types of actuators can only produce motion in one direction, generally only have one fluid port connecting the system and actuator, and rely on an external force (or internal spring in the case of some single-acting cylinders) to return them to their original positions (Rabie, 2009). Table 3 compares the in-house artificial muscle (and when in an antagonistic pair) to a double-acting cylinder purchased from Bimba.

As can be seen from the table, the in-house muscles are much cheaper than hydraulic cylinder and have higher force-to-weight ratio. In addition, the muscles built at the mesoscale have the advantage of simple construction, compactness, and easy integration into a robotic system.

Despite of similar static behavior, we believe, using muscles in hydraulic environment will give user more control over its stiffness and larger pressure and force

Table 3. Comparison of in-house fluidic artificial muscle and double-acting Bimba cylinder

	Fluidic artificial muscle (in-house)	Double-acting cylinder (Bimba) (Bimba: Pneumatic cylinders, n.d)
Size	1/8″ diameter and 4″ long	5/16″ bore and 4″ long
Stroke	25.4 mm	25.4 mm
Dry weight	0.0179 N (0.0359 N for pair)	0.2179 N
Maximum force at 100 psi	35.5858 N	34.1179 N
Maximum force-to-weight ratio	1990 (995 for pair)	157
Cost	US$ 0.96 (US$1.92 for pair)	US$21.09

bandwidth (Focchi et al., 2010). Using water as the working fluid as opposed to air has also been shown to have better load variations and hence improved control (Focchi et al., 2010). Also the energy cost of compressing a fluid is lower than compressing air. Using water or oil can also be beneficial for underwater robotic applications where the surrounding fluid can be used as the reservoir.

The model developed was able to predict muscle performance in static conditions. This model can be modified to include nonlinear dynamic behavior of the muscle. This can be achieved by incorporating variable stiffness term in the model.

Future work

In the future, the static model will incorporate more artificial muscle properties such as a factor to account for the stiffness of the mesh, and the viscoelastic properties of the inner latex/rubber tubing to attain a more accurate representation of the muscles. Furthermore, a series of dynamic tests will be performed on HAMs and PAMs. These tests will provide the most insight into the main differences in operation of the two actuators. Once these experiments have been performed, a dynamic model of hydraulic and pneumatic operation will be developed.

Some drawbacks of PAMs include the compressibility of the working fluid, air, and the amount of damping. These characteristics result in poorer dynamic response, as well as undesired oscillations of the actuators, respectively (Ahn and Chau, 2007; Klute et al., 2002). We hypothesize that utilizing oil as the working fluid, instead of air, will reduce the aforementioned issues of PAMs and yield better dynamic performance in general. Since oil is more viscous than air, using oil as the operating fluid could inherently help damp out the undesired oscillations that occur in PAMs. Response time could also potentially be improved significantly as traditional hydraulic systems tend to have response times about 50 times faster than equivalent pneumatic systems (Blackburn, 1960). The overall system efficiency has the potential to be increased greatly, as traditional pneumatic systems are rarely over 30% efficient due to the constant compressing of the working fluid, while their hydraulic counterparts are seldom over 60% efficient (Blackburn, 1960).

References

Ahn K and Chau NH (2007) Intelligent phase plane switching control of a pneumatic muscle robot arm with magneto-rheological brake. *Journal of Mechanical Science and Technology* 21(8): 1196–1206.

Beullens TH (1989) *Hydraulic or pneumatic drive device*. US patent 4,841,845.

Bimba: Pneumatic Cylinders (n.d.) Available at: http://www.bimba.com/Products/OriginalLineCylinders/

Blackburn JF (1960) *Fluid Power Control*. Cambridge: MIT Press.

Caldwell DG, Razak A and Goodwin M (1993) Braided artificial muscle actuators. In: *Proceedings of 3rd IFAC symposium on intelligent autonomous vehicles*, Southampton, UK, pp.507–512.

Chang X and Lilly JH (2003) Fuzzy control for pneumatic muscle tracking via evolutionary tuning. *Journal of Intelligent Automation and Soft Computing* 9(4): 227–244.

Chen Y, Yin W, Liu Y, et al. (2011) Structural design and analysis of morphing skin embedded with pneumatic muscle fibers. *Smart Materials and Structures* 20: 085033.

Chou CP and Hannaford B (1996) Measurements and modeling of McKibben pneumatic artificial muscles. *IEEE Transactions on Robotics and Automation* 12(1): 90–102.

Daerden F (1999) *Conception and realization of pleated pneumatic artificial muscles and their use as compliant actuation elements*. PhD Thesis, Vrije Universiteit Brussel, Belgium.

Daerden F and Lefeber D (2001) The concept and design of pleated pneumatic artificial muscles. *International Journal of Fluid Power* 2(3): 41–50.

Daerden F and Lefeber D (2002) Pneumatic artificial muscles: actuators for robotics and automation. *European Journal of Mechanical and Environmental Engineering* 47(1): 10–21.

Davis S, Tsagaraksi N, Canderle J and Caldwell DG (2003) Enhanced modeling and performance in braided pneumatic muscle actuators. *International Journal of Robotics Research* 22(3-4): 213–227.

Davis S and Caldwell DG (2006) Braid effects on contractile range and friction modeling in pneumatic muscle actuators. *International Journal of Robotics Research* 25(4): 359–369.

Ferris DP, Czerniecki JM and Hannaford B (2005) An ankle-foot orthosis powered by artificial pneumatic muscles. *Journal of Applied Biomechanics* 21(2): 189–197.

Fluidic Muscle DMSP/MAS (n.d.) From FESTO. Available at: http://www.festo.com/cms/en-us_us/2498.htm

Focchi M, Guglielmino E, Semini C, et al. (2010) Water/air performance analysis of fluidic muscle. *IEEE/RSJ International Conference on Intelligent Robots and Systems* 2194–2199.

Ho HW, Luk BL, Bradbeer RS, Yeung LF, Zhang HJ and Mould M (2000) The design of a hydraulically powered leg for an underwater six-legged robot. Mechatronics and Machine Vision J. Billingsley (Ed. Baldock) Hertfordshire U.K.: Research Studies 263–274.

Immega G and Kukolj M (1990) *Axially contractible actuator*. US patent 4,939,982.

Immega GB (1986) ROMAC muscle powered robots. Technical report MS86–777, Society of Manufacturing Engineers Dearborn.

Immega GB (1987) ROMAC actuators for micro robots. In: *IEEE micro robotics and teleoperators workshop* 9th November, Hyannis, MA.

Klute GK and Hannaford B (2000) Accounting for elastic energy storage in Mckibben artificial muscle actuators. *Journal of Dynamic Systems, Measurements and Control*, 122(2): 386–388.

Klute GK, Czerniecki JM and Hannaford B (2002) Artificial muscles: actuators for biorobotic systems. *The International Journal of Robotics Research* 21(4): 295–309.

Kothera CS, Woods BKS, Sirohi J, Wereley NM and Chen PC (2010) Fluid-driven artificial muscles as mechanisms for controlled actuation, United States Patent No. 7,837,144.

Ku, KKK and Bradbeer, RS (2006) Static Model of the Shadow Muscle under Pneumatic Testing. *Proceedings of the 4th Regional Inter-University Postgraduate Electrical and Electronics Engineering Conference* Macau, PRC, 13-14 July.

Ku KKK, Bradbeer RS, Lam KKY, Yeung LF and Li RCW (2009) *A novel actuator for underwater robots IEEE Journal of Oceanic Engineering* 34(3): 331–342.

Lee YK and Shimoyama I (1999) A skeletal framework artificial hand actuated by pneumatic artificial muscles. *Proceedings of the IEEE International Conference on Robotics and Automation* 2: 926–931.

Lilly JH (2003) Adaptive tracking for pneumatic muscle actuators in bicep and tricep configurations. *IEEE Transactions on Neural systems and rehabilitation engineering* 11: 333–339.

Nakamura T, Saga N and Yaegashi K (2003) Development of a pneumatic artificial muscle based on biomechanical characteristics. *IEEE International Conference on Industrial Technology* 2: 729–734.

Noritsugu T and Tanaka T (1997) Application of rubber artificial muscle manipulator as a rehabilitation robot. *IEEE/ASME Transactions on Mechatronics* 2(4): 259–267.

Paynter HM (1998) *High-pressure fluid-driven tension actuators and methods for constructing them*. US patent 4,751,869.

Philen M (2011) Force tracking control of fluidic flexible matrix composite variable stiffness structures. *Journal of Intelligent Material Systems and Structures* 22(1): 31–43.

Rabie MG (2009) *Fluid Power Engineering*. New York: McGraw-Hill Companies, Inc.

Reynolds DB, Repperger DW, Phillips CA, Bandry G (2003) Modeling the dynamic characteristics of pneumatic muscle. *Annals of Biomedical Engineering*, 31: 310–317.

Robinson RM, Kothera CS, Woods BKS, et al. (2011) High specific power actuators for robotic manipulators. *Journal of Intelligent Material Systems and Structures* 22(13): 1501–1511.

Ryu D, Moon KW, Nam H, et al. (2008) Micro hydraulic system using slim artificial muscles for a wearable haptic glove. In: *Proceedings of the IEEE international conference on intelligent robots and systems*, Nice, France, pp.3028–3033.

Schulte HF (1961) The characteristics of the Mckibben artificial muscle. The Application of External Power in Prosthetics and Orthotics, National Academy of Sciences–National Research Council, Lake 874: 94–115.

Shadow Robot Company (n.d.) 30 mm Air Muscle – Specification. Available at: http://www.shadowrobot.com/

Shan Y, Philen M, Lotfi A, et al. (2009) Variable stiffness structures utilizing fluidic flexible matrix composites. *Journal of Intelligent Material Systems and Structures* 20(4): 443–456.

Solano B and Rotinat-Libersa C (2011) Compact and lightweight hydraulic actuation system for high performance millimeter scale robotic applications: modeling and experiments. *Journal of Intelligent Material systems and Structures* 22: 1479–1487.

Tondu B, Ippolito S and Guiochet J (2005) A seven degree of freedom robot arm driven by pneumatic artificial muscles for humanoid robot. *The International Journal of Robotics Research* 24(4): 257–274.

Tondu B and Lopez P (1997) The McKibben muscle and its use in actuating robot-arms showing similarities with human arm behaviour. *Industrial Robot* 24(6): 432–439.

Tondu B and Lopez P (2000) Modeling and Control of McKibben Artificial Muscle Robot Actuators. *IEEE Control Systems Magazine*, 20(2): 15–38.

Tri VM, Tjahjowidodo T, Ramon H and Van Brussel H (2009) Non-local Memory Hysteresis in A Pneumatic Artificial Muscle Proceedings of the 17th Mediterranean Conference on Control and Automation, Thessaloniki, Greece, 640–645.

Tri VM, Tjahjowidodo T, Ramon H and Van Brussel H (2010) A new approach to modeling hysteresis in a pneumatic artificial muscle using the Maxwell-slip model. *IEEE/ASME Transaction on Mechatronics*, 16(1): 177–186.

Vanderborght B, Verrelst B, Ham RV, et al. (2006) Controlling a bipedal walking robot actuated by pleated pneumatic artificial muscles. *Journal Robotica* 24(4): 401–410.

Varga Z and Moučka M (2009) Mechanics of pneumatic artificial muscle. *Journal of Applied Science in the Thermodynamics and Fluid Mechanics* 3(2) (http://astfm.tul.cz/journal/year-2009/2st-issue/)

Waycaster G, Wu S-K and Shen X (2011) Design and control of a pneumatic artificial muscle actuated above-knee prosthesis. *Journal of Medical Devices* 5(1): 031003.

Wereley N, Kothera C, Bubert E, et al. (2009) Pneumatic artificial muscles for aerospace applications. In: *17th structures, structural dynamics, and materials conference* Palm Spring, California.

Wickramatunge KC and Leephakpreeda T (2010) Study on mechanical behavior of pneumatic artificial muscle. *International Journal of Engineering Science* 48: 188–198.

Wigging MB, Sawicki GS and Collins SH (2011) An exoskeleton using controlled energy storage and release to aid ankle propulsion. *IEEE International Conference on Rehabilitation Robotics* 1–5.

Winters JM (1995) Braided artificial muscles: mechanical properties and future uses in prosthetics/orthotics. In: *Proceedings of the RESNA 13th annual conference* Washington DC, 173–174.

Wisse M and Frankenhuyzen JV (2003) Design and construction of Mike; 2D autonomous biped based on passive dynamic walking. In: *Proceedings of international symposium on adaptive motion of animals and machines* Kyoto, Japan, p.3.

Woods BKS, Kothera CS and Wereley NM (2011) Wind tunnel testing of a helicopter rotor trailing edge flap actuated via pneumatic artificial muscles. *Journal of Intelligent Material Systems and Structures* 22(13): 1513–1528.

Yarlott JM (1972) *Fluid actuator*. US patent 3,645,173.

Yerkes N and Wereley N (2008) Pneumatic artificial muscle activation for trailing edge flaps. In: *46th AIAA aerospace*

sciences meeting and exhibit, AIAA paper 2008-1418 7-10 January, Reno, Nevada.

Yoshinada H, Yamazaki T, Suwa T, et al. (1991) Seawater hydraulic actuator system for underwater manipulator. In: *Proceedings of 5th international conference advanced robot*, Pisa, Italy, vol. 2, pp.1330–1335.

Appendix 1

Notation

Symbol	Definition	Value	Units
F	Force output	—	N
l	Length of one side of a trapezoid of mesh	1	mm
P	Pressure of fluid inside muscle	—	psi
V	Volume of muscle	—	mm^3
L	Length of muscle	—	mm
θ	Mesh angle	—	deg
D	Diameter of muscle	—	mm
C	Circumference of muscle	—	mm
B	Length of one strand of mesh	25	mm
N	Number of turns one strand makes	1	—
G	Distance between two mesh nodes	—	mm
W_B	Thickness of a mesh strand	0.25	mm
N_C	Number of nodes around a muscle	18	—
D_o	Diameter of muscle when $\theta = 90^{\circ}$	7.958	mm
$F_{friction}$	Force from friction	—	N
$S_{contact}$	Total area of overlapping strands	—	mm^2
f_s	Friction coefficient	0.1	—
E	Contraction ratio	—	—